Applied Energy 208 (2017) 480–494

Contents lists available at ScienceDirect

Applied Energy

journal homepage: www.elsevier.com/locate/apenergy

Hierarchical microgrid energy management in an office building

Xiaolong Jin[a,b], Jianzhong Wu[a,*], Yunfei Mu[b,*], Mingshen Wang[b], Xiandong Xu[a], Hongjie Jia[b]

[a] Institute of Energy, School of Engineering, Cardiff University, Cardiff CF24 3AA, UK
[b] Key Laboratory of Smart Grid of Ministry of Education, Tianjin University, Tianjin 30072, China

HIGHLIGHTS

- A hierarchical microgrid energy management method in an office building is proposed.
- An office building is modelled as a virtual energy storage system (VESS).
- A V2B control strategy is developed to dispatch the EVs as a flexible resource.
- The VESS and the EVs are coordinated and dispatched in two different time scales.

ARTICLE INFO

Keywords:
Microgrid
Virtual energy storage system
Vehicle-to-Building
Electric vehicle
Energy management

ABSTRACT

A two-stage hierarchical Microgrid energy management method in an office building is proposed, which considers uncertainties from renewable generation, electric load demand, outdoor temperature and solar radiation. In stage 1, a day-ahead optimal economic dispatch method is proposed to minimize the daily Microgrid operating cost, with the virtual energy storage system being dispatched as a flexible resource. In stage 2, a two-layer intra-hour adjustment methodology is proposed to smooth the power exchanges at the point of common coupling by coordinating the virtual energy storage system and the electric vehicles at two different time scales. A Vehicle-to-Building control strategy was developed to dispatch the electric vehicles as a flexible resource. Numerical studies demonstrated that the proposed method is able to reduce the daily operating cost at the day-ahead dispatch stage and smooth the fluctuations of the electric power exchanges at the intra-hour adjustment stage.

1. Introduction

Increasing attention is being paid to technologies in renewable energy and energy efficiency improvement due to the rapid growth of global energy use and environmental deterioration [1,2]. According to the International Energy Agency, energy consumption of buildings occupies about 32% of the global energy use and they are responsible for about 30% of the total end-use and energy-related CO_2 emissions [3]. As a result, a number of regions and countries have taken specific initiatives to facilitate a high penetration of renewable generation and the low energy consumption technologies in their building sectors, including the European Union [4], the United States [5] and China [6–9]. In China, the building sector currently accounts for 27.6% of the total energy use and it is estimated to reach 35% by 2020 [6,7]. The Chinese government has paid attention to the retrofits and renovations of the existing buildings, and provided financial support for the energy management in large public buildings [8,9]. Therefore, as the major power consumers at demand side, buildings represent a great potential contributor for reducing the energy consumption and relieving power imbalance of the electric grid.

Aiming to facilitate a high penetration of renewable generation and the low energy consumption technologies at the demand side, there is significant development of low-carbon buildings integrated with renewable generation [10]. However, renewable generation is usually intermittent, uncertain and uncontrollable, which induces power mismatches between power demand and supply for low-carbon buildings [10].

Microgrids provide an opportunity and a desirable infrastructure for facilitating integration of intermittent renewable generation in low-carbon buildings [11]. Microgrids can increase the penetration of intermittent renewable generation and provide an economical energy supply for the low-carbon buildings by utilizing advanced energy management technologies and intelligent communication technologies [12]. The fluctuations of the electric power exchanges at the point of

* Corresponding authors.
E-mail addresses: xljin@tju.edu.cn (X. Jin), wuj5@cardiff.ac.uk (J. Wu), yunfeimu@tju.edu.cn (Y. Mu), wangmingshen@tju.edu.cn (M. Wang), xux27@cardiff.ac.uk (X. Xu), hjjia@tju.edu.cn (H. Jia).

http://dx.doi.org/10.1016/j.apenergy.2017.10.002
Received 31 July 2017; Received in revised form 19 September 2017; Accepted 1 October 2017
Available online 14 October 2017

Nomenclature

Abbreviations

VESS	virtual energy storage system
PCC	point of common coupling
EC	electric chiller
V2B	Vehicle-to-Building
SOC	State-of-Charge
M1	passenger vehicle, four wheels up to 8 seats in addition to the driver's seat
HBW	Home Based Work
EV	electric vehicle

Sets and indices

T, t	set of indexes of the dispatch time slots
J, j	set of indexes of the EVs

Parameters and constants

C_{ph}, C_{se}	real-time electricity purchasing/selling prices ($/kWh)
P_{el}	electric load of the Microgrid (kW)
P_{PV}	electric power generated by photovoltaic system (kW)
U_{wall}, U_{win}	heat transfer coefficient of the wall/window of the building [W/(m^2·K)]
$F_{wall,j}$	the area of the total wall surface at the jth wall orientation (m^2)
$F_{win,j}$	the area of the total window surface at the jth wall orientation (m^2); It is assumed that the total window surfaces are distributed in the south, west, north and east orientations of the walls in a building uniformly
T_{out}	outdoor temperature (°C)
τ_{win}	the glass transmission coefficient of the windows
SC	the shading coefficient of the windows
α_w	absorbance coefficient of the external surface of the wall
$\dot{Q}_{in}$	internal heat gains from people, appliances and lighting (kW)
ρ, C, V	the density (kg/m^3), specific heat capacity [J/(kg·°C)] and volume of the air (m^3) in the building
$R_{se,j}$	the external surface heat resistance for convection and radiation of the external wall j (m^2·K/W)
$I_{T,j}$	the total solar radiation on the walls/windows surface at the j-wall orientation (kW/m^2)
EER_{EC}	energy efficiency ratio of the EC
ρ_{PV}	maintenance cost of the photovoltaic system ($/kWh)
ρ_{EC}	maintenance cost of the EC ($/kWh)
$t_{in,\ j}$, $t_{out,\ j}$	plug-in/plug-out time of EV j
$P_{j,t}^{V,c}$, $P_{j,t}^{V,d}$	the rated charging and discharging power of EV j at time t (kW)
$\underline{P}_{j,t}^{V}$, $\overline{P}_{j,t}^{V}$	the lower and upper power output limits of the EV j at time t (kW)
$SOC_{j,d,home}$	the expected SOC when EV j leaves home
C_e	the EV energy consumption per kilometer (kWh/km)
D	EV's daily travelling distance (km)
Cap	the battery capacity of M1 EV (kW)
$Cap_{\min}$	the minimum battery capacity of M1 EV (kW)
$Cap_{\max}$	the maximum battery capacity of M1 EV (kW)
$\eta_{j,c}$, $\eta_{j,d}$	the charging and discharging efficiency of EV j
$\overline{SOC}_j^V$	the upper limit of the SOC of EV j
$\underline{SOC}_j^V$	the lower limit of the SOC of EV j
$\overline{Q}_{EC}$	the upper limit of the cooling power output of the EC (kW)
$\overline{T_{in}}$, $\underline{T_{in}}$	the upper and lower limits of the indoor temperature set-points of the building (°C)
$\overline{P_{ex}}$, $\underline{P_{ex}}$	the upper and lower limits of electric power exchange with the external grid of the building (kW)

Variables

P_{ex}	electric power exchange with the external grid (kW)
P_{EC}	electric power consumption by the EC (kW)
$\dot{Q}_{EC}$	cooling power generated by the EC (kW)
$\dot{Q}_{wall}$	heat transfer through the external walls (kW)
$\dot{Q}_{win}$	heat transfer across the windows (kW)
$\dot{Q}_{sw}$	heat contribution due to the solar radiation on the opaque surface of the external walls (kW)
$\dot{Q}_{sg}$	the whole solar radiation transmitted across the windows (kW)
$\dot{Q}_{cl,building}$	cooling load of the Microgrid with VESS being dispatched (kW)
$\dot{Q}'_{cl,building}$	cooling load of the Microgrid without VESS being dispatched (kW)
$SOC_{in,\ j}$	the initial SOC of EV j
$SOC_{j,d,office}$	the minimum expected SOC at t_{out} of EV j
$D_{h\text{-}w}$	the EV's travelling distance from home to work (km)
$P_{j,t}^{V}$	the real-time power output of EV j at time t (kW), with negative (positive) value representing the charging (discharging) process
$P_{\mathrm{V2B},t}$	the real-time power output of the V2B system at time t (kW)
$P_{\mathrm{V2B},t}^{tar}$	the target power output of the V2B system at time t (kW)
$P_{\mathrm{V2B},t}^{upper}$	the upper boundary of the power output of the V2B system at time t (kW)
$P_{\mathrm{V2B},t}^{lower}$	the lower boundary of the power output of the V2B system at time t (kW)
T_{in}	indoor temperature set-point (°C)

common coupling (PCC) of a Microgrid can also be smoothed by coordinating and optimizing the operation of various energy sources and energy loads of the Microgrid [13,14]. Therefore, Microgrid energy management in buildings is attracting more and more attentions in recent years.

Studies have been carried out to investigate the Microgrid energy management methods in a commercial building. The operational performance of a Microgrid in a building in Hong Kong was studied considering operating cost and environmental constraints [10]. A multi-objective dispatch model was proposed in [15] to minimize the daily operating cost and the pollutants emission. An electric chiller (EC) was used as the cooling system of a building in [16] and the electric power consumption of the EC was dispatched using a nonlinear programming method for cost saving. In [17], the electric power consumption of an EC was dispatched in the dynamic economic dispatch process with the discrete EC operating constraints. As a flexible resource, the integration of electric vehicles (EVs) to the building is creating new opportunities for the Microgrid energy management [18,19]. EVs have a certain flexibility to shift their electricity consumption in time and facilitate the integration of intermittent renewable generation [20,21]. A Microgrid energy management method in an office building was proposed in [22] to reduce the impact of EV charging on the external grid with different charging strategies being considered. In [23], a Vehicle-to-Building (V2B) operational model was proposed for the EVs to reduce the total energy cost of a Microgrid in a building.

The existing research work has made good contributions to the Microgrid energy management in a building. However, the flexibility of the building with heat inertia hasn't been fully explored in the Microgrid energy management. As the major power consumer of the Microgrid, a building can perform as a distributed thermal storage to

participate in the energy management. The building heating/cooling demand can be adjusted in the energy management process without disturbing the temperature comfort level due to the building thermal mass [24,25]. Accordingly, the power consumption of the heating/cooling system can be dispatched in the energy management process considering the indoor temperature comfort zone.

Furthermore, the existing research work mainly focuses on reducing the Microgrid operating cost. The fluctuations of the electric power exchanges at the PCC will pose significant challenges on the external grid [13], such as voltage constraint violations and equipment thermal overloading. A Microgrid will be charged for the reserve services to compensate power imbalances, which results from the fluctuations of the electric power exchanges at the PCC [26]. Therefore, smoothing the fluctuations of the electric power exchanges at the PCC will benefit both the external grid and the Microgrid. Both operating cost reduction and smoothing fluctuations of the electric power exchanges at the PCC should be considered in the Microgrid energy management.

Moreover, due to the heat inertia of a building, heating/cooling energy exchange between indoor and outdoor environment is much slower compared to electric EV charging/discharging. Hence, the response characteristics of the building and EVs are different. In this case, the two flexible resources should be managed and coordinated at different time scales to make the energy management more efficient. However, different response characteristics and different dispatch time scales of the building and the EVs are not well considered in previous studies.

This paper studies the energy management method for a Microgrid in an office building operating in the grid-connected mode. The main contributions are summarized as follows:

(1) A novel two-stage hierarchical Microgrid energy management method in an office building is proposed, which consists of a day-ahead optimal economic dispatch stage and a two-layer intra-hour adjustment stage. Two objectives, i.e., reducing the daily operating cost and smoothing the fluctuations of the electric power exchanges at the PCC, can be achieved with the proposed energy management method. The proposed energy management method benefits both the Microgrid and the external grid.
(2) An office building is simplified to a lumped thermal mass and modelled as a simplified thermal storage system, namely the virtual energy storage system (VESS). The VESS is dispatched as a flexible resource in the Microgrid energy management.
(3) A V2B control strategy is proposed to dispatch the EVs as another flexible resource in the Microgrid energy management method. The proposed strategy can control the charging/discharging power of the EVs considering their plug-in and plug-out times, initial State-of-Charge (SOC) statuses and energy demands. A forced-charging boundary is further considered in the V2B control strategy to guarantee sufficient energy in the EV battery for user's travel from work to home.
(4) The VESS and the EVs under V2B control are dispatched at two different time scales considering their different response characteristics at the intra-hour stage, which makes the energy management more efficient.

2. Methods

2.1. Configuration of the Microgrid in an office building

A Microgrid in an office building is adopted as the test system in this paper, as shown in Fig. 1. The Microgrid includes a photovoltaic system, an EC and a V2B system (The EVs under V2B control is abbreviated as V2B system in this paper). In the Microgrid, the electricity suppliers are the photovoltaic system and the external power grid. And the electricity consumers are the EC, the lighting and office appliances. Meanwhile, there is a balance between the cooling supply and demand. The building is the cooling consumer and the EC is the cooling supplier.

2.2. Model of virtual energy storage system

Considering a summer cooling scenario, a building is modelled as a single isothermal air volume [27]. The mathematical relationship among the indoor temperature set-point, cooling demand and outdoor temperature is established to investigate the thermal performance of a building by using the building thermal equilibrium equation, as shown in Eq. (1) [28].

$$\rho \times C \times V \times \frac{dT_{in}}{dt} = \dot{Q}_{wall} + \dot{Q}_{win} + \dot{Q}_{in} + \dot{Q}_{sw} + \dot{Q}_{sg} - \dot{Q}_{EC} \quad (1)$$

(i) $\dot{Q}_{wall}$ is calculated by summing the contribution of each wall of a building, as shown in Eq. (2). The roof of a building is accounted for as part of the external walls [29].
(ii) $\dot{Q}_{win}$ is calculated by summing the contribution of each window of a building, as shown in Eq. (3).
(iii) $\dot{Q}_{in}$ is the internal heat gains (kW).
(iv) $\dot{Q}_{sw}$ is calculated by summing the heat contribution due to solar radiation on each external wall (south, west, north and east

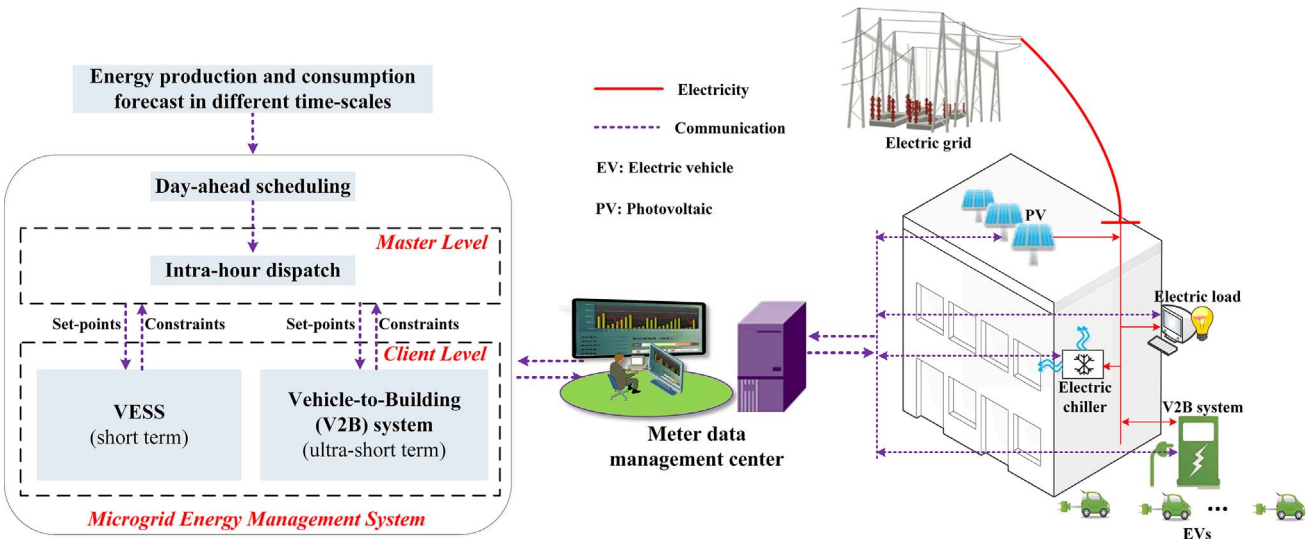

Fig. 1. Configuration of the hierarchical Microgrid management system.

orientations) according to the ISO 13790 [30], as shown in Eq. (4). Also, the external surface heat resistance for convection and radiation of the external wall j, $R_{se,j}$, is considered in Eq. (4). A typical method to calculate the $R_{se,j}$ is given in [31], which takes both radiation and convection terms into account.

(v) $\dot{Q}_{sg}$ is calculated according to Eq. (5). It is assumed that the total windows surfaces are distributed in the south, west, north and east orientations of the walls in a building uniformly [32].

(vi) $\dot{Q}_{EC}$ is the cooling power generated by the cooling equipment (kW).

$$\dot{Q}_{wall} = \sum_{j\in J} U_{wall} \times F_{wall,j} \times (T_{out} - T_{in}) \tag{2}$$

$$\dot{Q}_{win} = \sum_{j\in J} U_{win} \times F_{win,j} \times (T_{out} - T_{in}) \tag{3}$$

$$\dot{Q}_{sw} = \sum_{j\in J} \alpha_w \times R_{se,j} \times U_{wall} \times F_{wall,j} \times I_{T,j} \tag{4}$$

$$\dot{Q}_{sg} = \sum_{j\in J} \tau_{win} \times SC \times F_{win,j} \times I_{T,j} \tag{5}$$

$I_{T,j}$ is determined according to the method presented by Duffie and Beckman [33], which is a commonly used method to calculate the total solar radiation on a tilted surface [34]. It can be calculated as sum of various types of solar radiation, i.e., beam, diffuse and reflected radiation, as shown in Eq. (6):

$$I_T = I_b \times R_b + I_d \times \left(\frac{1+\cos\beta}{2}\right) + I \times \rho_g \times \left(\frac{1-\cos\beta}{2}\right) \tag{6}$$

where I_b, I_d and I represent beam, diffuse and total radiation on horizontal surface respectively (kW/m^2); ρ_g is the ground reflectance and is taken as 0.2 in the present study [34]; R_b is geometric factor which is defined as the ratio of beam radiation on a tilted surface to that on a horizontal surface. R_b is expressed as:

$$R_b = \frac{\cos\theta}{\cos\theta_z} \tag{7}$$

where θ and θ_z are incidence and zenith angles.

The model of VESS is developed considering the thermal performance of the building. The basic idea of the VESS is that the cooling demand of the building can be adjusted in the energy management process without disturbing the temperature comfort level due to the thermal mass of the building. Therefore, the cooling energy generated by the EC is stored in the building when the electricity price is low, i.e., the EC is started in advance or the power consumption of the EC is increased. In that case, the VESS is charged seen from the Microgrid, i.e., $\dot{Q}'_{cl,building} < \dot{Q}_{cl,building}$. In the same way, the cooling energy generated by the EC is discharged in the building when the electricity price is high, i.e., the EC is shut down in advance or the power consumption of the EC is decreased. In that case, the VESS is discharged seen from the Microgrid, i.e., $\dot{Q}'_{cl,building} > \dot{Q}_{cl,building}$. The charging/discharging power of the VESS, as shown in Eq. (8), is obtained following Eq. (1). The indoor temperature comfort zone and temperature set-point are considered in the model of VESS to maintain the customer comfort level.

$$\dot{Q}_{VESS,t} = \dot{Q}'_{cl,building,t} - \dot{Q}_{cl,building,t} \tag{8}$$

The office building is modelled as a steady-state model of the VESS. The steady-state model is used in the Microgrid energy management in the office building with a large simulation time step. And the indoor temperature set-points are adjusted to dispatch the VESS for energy management of the office building. The real indoor temperatures will be values fluctuating around the indoor temperature set-points. How to develop building model considering the dynamics of the building and capture the dynamic indoor temperatures by building simulation methods with small simulation time step will be the future research work.

2.3. The Vehicle-to-Building (V2B) model

The V2B model consists of three models: (1) the EV battery model; (2) the model of EV mobility behaviour; and (3) the operation constraints of the EV. The generic EV battery model developed in [20,35] is used to obtain the relationship between the SOC and the charging/discharging behaviours of the EVs.

2.3.1. EV battery model

Since this paper focuses on the EVs in an office building, the type of the EVs is determined as M1 with Home Based Work (HBW) transportation pattern according to a depth survey of the worldwide EV battery market [36]. According to [36], the probability density function (*pdf*) of EV battery capacity (*Cap*) of M1 EV is defined as the truncated Gamma distribution, as shown in Eq. (9).

$$\begin{cases} f(Cap,\alpha,\beta) = \begin{cases} 0, -\infty < Cap < Cap_{\min} \quad \text{or} \quad Cap_{\max} < Cap < +\infty \\ \frac{f_0(Cap,\alpha,\beta)}{\int_{Cap_{\min}}^{Cap_{\max}} f_0(Cap,\alpha,\beta)dCap}, \quad Cap_{\min} \leqslant Cap \leqslant Cap_{\max} \end{cases} \\ f_0(Cap,\alpha,\beta) = \frac{1}{\beta^\alpha \Gamma(\alpha)} Cap^{\alpha-1} e^{-\frac{Cap}{\beta}} \end{cases} \tag{9}$$

α and β are the shape parameter and the scale parameter of the *pdf* of Gamma distribution. The *pdf* of battery capacity of M1 EV is shown in Table 1.

2.3.2. Model of EV mobility behaviour

It is assumed that all the EVs investigated in this paper are charged at home. They are charged to their expected SOCs ($SOC_{d,home}$) before travelling to satisfy their energy demands travelling from home to work. The $SOC_{d,home}$ varies uniformly in the range of [80%, 90%] to satisfy the travelling demands of the EV users and maintain the life time of a battery from overcharge [21]. It is assumed that SOC drops linearly with the travel distance. The SOC of an EV when it arrives at the office (SOC_{in}) is calculated by Eq. (10). Since the EVs are charged to $SOC_{d,home}$ at home, the minimum expected SOC at the plug-out time when they leave the office ($SOC_{d,office}$) is set to be the same as the SOC_{in}.

$$SOC_{in} = SOC_{d,home} - \frac{D_{h-w} \times C_e}{Cap} \tag{10}$$

The distribution of M1 EV of the C_e is shown in Table 2 [36]; $D_{h\text{-}w}$ is assumed to be half of the EV's daily travelling distance (D) according to HBW EVs' mobility behaviour [36]. $D_{h\text{-}w}$ is calculated by Eq. (11).

$$D_{h-w} = D/2 \tag{11}$$

D basically follows a Normal distribution, as shown in Eq. (12) [37].

$$f(D,\mu_d,\sigma_d) = \frac{1}{\sigma_d\sqrt{2\pi}} e^{-(D-\mu_d)^2/2\sigma_d^2} \tag{12}$$

μ_d is the mean value of daily travelling distance; σ_d is the standard deviation. For HBW vehicles, the μ_d is 35.9 km and the σ_d is 19.6 km [38].

The plug-in time (t_{in}) when the EVs arrive at the office and the plug-out time (t_{out}) when the EVs leave the office are determined based on the office time, which are assumed to follow the Normal distribution [18]. Based on the information supplied by the battery characteristics and mobility behaviours, the Monte Carlo simulation method is used to

Table 1
The *pdf* of battery capacity of M1 EV [36].

Distribution	Gamma
Parameter	α = 4.5
	β = 6.3
Max (kWh)	72.0
Min (kWh)	10.0

Table 2
Distributions of M1 EV energy consumption per kilometer [36].

C_e (kWh/km)	Distribution(p.u.)
0.05–0.10	0.05
0.10–0.15	0.35
0.15–0.20	0.45
0.20–0.25	0.15

generate the *Cap*, SOC_{in}, t_{in} and t_{out} for all the EVs.

2.3.3. Operation constraints of the EV

An individual EV is able to serve as an energy storage unit with its rapid charging and discharging characteristics. In order to dispatch the EVs under the V2B control effectively, the charging and discharging power is defined as the power output of the EV, and a negative (positive) value of the power output represents the charging (discharging) process. The operation area of an individual EV is shown in Fig. 2.

For an individual EV, the operation area (the shaded area shown in Fig. 2) is limited by the boundaries of power output and the boundaries of state of charge (SOC). Points *A*, *B*, *C*, *D*, *E* and *F* are used to describe the upper and lower boundaries of the operation area:

- The upper boundary of the operation area follows the path of '*A-B-C*'. Following this path, EV *j* is charged at the rated charging power as soon as it plugs in at t_{in} until the SOC upper limit ($\overline{SOC}_j^V$) is reached (from point *A* to *B*). The SOC of EV *j* is constant and the power output of EV *j* is zero from point *B* to *C*.
- The lower limit of the operation area follows the path of '*A-D-E-F*'. Following this path, EV *j* is discharged at the rated discharging power as soon as it plugs in at t_{in} until the SOC lower limit ($\underline{SOC}_j^V$) is reached (from point *A* to *D*). The SOC of EV *j* is constant and the power output of EV *j* is zero from point *D* to *E*.
- In order to guarantee sufficient energy in the EV battery for user's travel from work to home at the plug-out time, a forced-charging boundary is proposed in the V2B control strategy. When the charging/discharging path hits the forced-charging boundary (from points *E* to *F*), EV *j* starts to charge with the rated charging power to achieve the minimum expected SOC ($SOC_{j,d,office}$) at t_{out}. When the charging/discharging path hits the forced-charging boundary, the EV turns into an uncontrollable load and starts to charge at the rated charging power until the plug-out time.

It is worth noting that, the charging boundaries of '*A-B*' and '*A-D*' are natural boundaries constrained by the rated charging and discharging power of an individual EV; the charging boundaries of '*D-E*' and '*B-C*' are natural boundaries constrained by the EV battery maintenance constraints, as shown in Eq. (13); the charging boundary of '*E-F*' is a forced boundary to guarantee the minimum expected SOC ($SOC_{j,d,office}$) at t_{out}; and the charging boundary of '*C-F*' is a flexible boundary with acceptable range of $SOC_{j,d,office}$, as shown in Eq. (14).

$$\underline{SOC}_j^V \leqslant SOC_{j,t} \leqslant \overline{SOC}_j^V \tag{13}$$

$$SOC_{j,t_{out}} \geqslant SOC_{j,d,office} \tag{14}$$

The real-time power output of EV *j* is defined as $P_{j,t}^V$. The negative (positive) value of $P_{j,t}^V$ means that the EV is charging (discharging) at time *t*. Then the real-time SOC value ($SOC_{j,t}$) is determined by Eq. (15). The lower and upper power output limits of the EV *j* ($\underline{P}_{j,t}^V$ and $\overline{P}_{j,t}^V$) are described in Eq. (16).

$$SOC_{j,t} = SOC_{in,j} - \frac{\int_{t_{in,j}}^{t_{out,j}} P_{j,t}^V dt}{Cap_{j,t}^r}, \quad t_j \in [t_{in,j}, t_{out,j}] \tag{15}$$

$Cap_{j,t}^r$ is the revised EV battery capacity, which is determined by the actual EV battery capacity and the charging state, as shown in Eq. (17).

$$\begin{cases} \underline{P}_{j,t}^V = -P_{j,t}^{V,c}, \overline{P}_{j,t}^V = P_{j,t}^{V,d}, & t \in [t_{in,j}, t_{out,j}] \\ \underline{P}_{j,t}^V = \overline{P}_{j,t}^V = 0, & t \notin [t_{in,j}, t_{out,j}] \end{cases} \tag{16}$$

$P_{j,t}^{V,c}$ is assumed to be equal to $P_{j,t}^{V,d}$ in this paper. The EVs, which have hit the boundary of '*B-C*', are not allowed to charge. In that case, the lower power output limit ($\underline{P}_{j,t}^V$) is increased to zero. The EVs, which have hit the boundary of '*D-E*', are not allowed to discharge. In that case, the upper power output limit ($\overline{P}_{j,t}^V$) is decreased to zero. The EVs, which have hit the forced-charging boundary of '*E-F*', are forced to charge with the rated charging power. In that case, both the upper and lower power output limits will be changed to $-P_{j,t}^{V,c}$.

$$Cap_{j,t}^r = \begin{cases} Cap_j/\eta_{d,j}, & P_{j,t}^V > 0 \\ Cap_j, & P_{j,t}^V = 0 \\ Cap_j/\eta_{c,j}, & P_{j,t}^V < 0 \end{cases} \tag{17}$$

Then, the real-time power output of the V2B system ($P_{V2B,t}$), the upper boundary ($P_{V2B,t}^{upper}$) and the lower boundary ($P_{V2B,t}^{lower}$) of the $P_{V2B,t}$ under the V2B control are shown in Eq. (18).

$$\begin{cases} P_{V2B,t} = \sum_{j=1}^{N_t} P_{j,t}^V \\ P_{V2B,t}^{upper} = \sum_{j=1}^{m_t} (-P_{j,t}^{V,c}) + \sum_{j=1}^{n_t} \overline{P}_{j,t}^V \\ P_{V2B,t}^{lower} = \sum_{j=1}^{m_t} (-P_{j,t}^{V,c}) + \sum_{j=1}^{n_t} \underline{P}_{j,t}^V \end{cases} \tag{18}$$

N_t is the total number of EVs at time *t*; m_t is the number of EVs operating on the forced-charging boundary ('*E-F*') at time *t*; n_t is the number of the other EVs ($n_t = N_t - m_t$).

2.4. The hierarchical energy management method

2.4.1. Framework of the hierarchical Microgrid energy management method

The proposed hierarchical energy management method is illustrated in Fig. 3, which includes two stages: the day-ahead optimal dispatch stage that minimizes the daily Microgrid operating cost and the two-layer intra-hour adjustment stage that smooths the fluctuations of the electric power exchanges at the PCC. With the hourly electric load demand, outdoor temperature, solar radiation and the renewable generation forecasting values, the hourly schedules of the day-ahead dispatch stage over the n_1 time slots are obtained by using an optimal dispatch program.

Due to the forecasting errors of the renewable generation, electric load demand, outdoor temperature and solar radiation, mismatches exist in both day-ahead and intra-hour schedules of the electric power exchanges at the PCC. Therefore, a two-layer intra-hour adjustment stage is conducted to smooth the fluctuations of the electric power exchanges at the PCC in both short term (15 min) and ultra-short term (1 min). At the master layer, the optimal dispatch program is used to

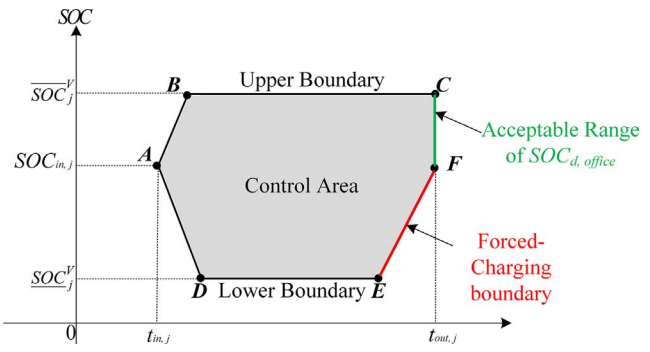

Fig. 2. The operation area of an individual EV.

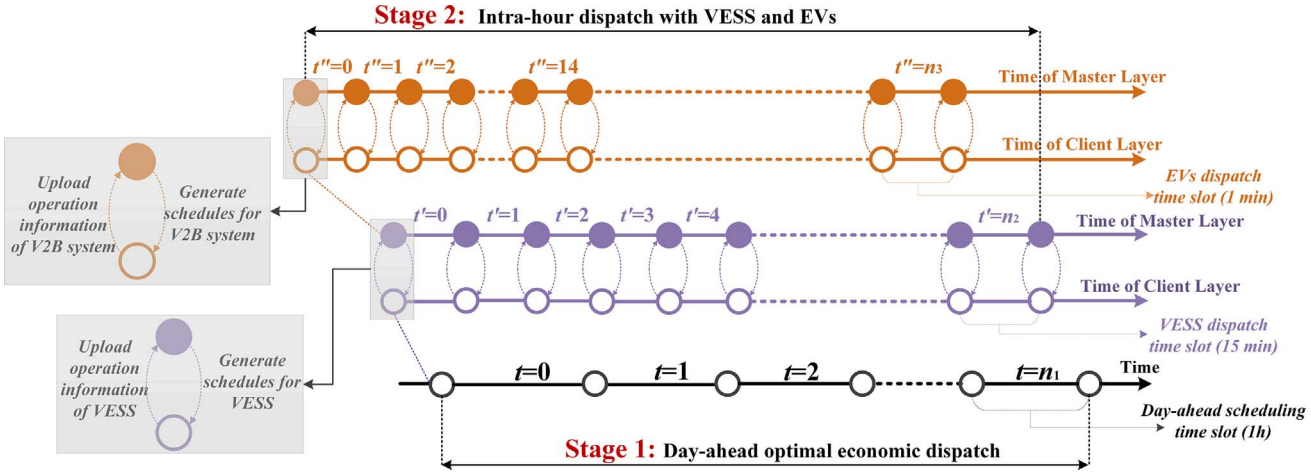

Fig. 3. Schematic illustration of the hierarchical energy management method.

generate operating schedules for the VESS (charging/discharging power of the VESS) and the V2B system (charging/discharging power of all EVs) over the n_2 time slots and n_3 time slots respectively. At the client layer, the operation information of the VESS (occupied hours of the building and the indoor temperature comfort zone) as well as the upper and lower boundaries of power output of the V2B system are uploaded to the master.

Due to the thermal inertia of a building, the heating/cooling energy exchange between indoor and outdoor environment is much slower compared to the electric EV charging/discharging. Meanwhile, the charging and discharging of EVs are chemical and electromagnetic processes, without mechanical processes. Consequently, the EVs are characterized with quick response which makes them especially suitable to be dispatched in the ultra-short term [39]. Therefore, different dispatch intervals are set for the VESS (short dispatch interval in 15 min) and the V2B system (ultra-short dispatch interval in 1 min).

2.4.2. Microgrid energy management: stage 1

With the hourly electric load demand, outdoor temperature, solar radiation and the renewable generation forecasting values, the hourly schedules of the day-ahead dispatch stage over the horizon $T = \{0, \ldots, t, n_1\}$ are obtained using an optimal dispatch program. The optimization problem of stage 1 is formulated as follows:

- *Objective function*

The objective function is to minimize the daily Microgrid operating cost.

$$\min \sum_{\substack{t=0 \\ t\in T}}^{n_1} \left\{ \left(\frac{C_{ph,t} + C_{se,t}}{2} P_{ex,t} + \frac{C_{ph,t} - C_{se,t}}{2} |P_{ex,t}| \right) + (\rho_{PV} P_{PV,t} + \rho_{EC} P_{EC,t}) \right\} \tag{19}$$

The first term in Eq. (19) represents the cost for electricity purchase from the external grid; the second term is the maintenance cost of the photovoltaic and the EC.

- *Constraints*

(1) Electrical power balance:

$$P_{ex,t} + P_{PV,t} = P_{el,t} + P_{EC,t}\,, \quad \forall\, t \in T \tag{20}$$

(2) Cooling demand balance:

$$\dot{Q}_{EC,t} = EER_{EC} \times P_{EC,t} = \dot{Q}_{cl,building,t}\,, \quad \forall\, t \in T \tag{21}$$

(3) Building thermal equilibrium equation:

The finite difference equation is considered as the building thermal equilibrium constraint, as shown in Eq. (22).

$$\Delta t \Big[\sum_{j\in J} U_{wall} \times F_{wall,j} \times (T_{out,t} - T_{in,t}) + \sum_{j\in J} U_{win} \times F_{win,j} \times (T_{out,t} - T_{in,t}) + \sum_{j\in J} \alpha_w \times R_{se,j} \times U_{wall} \times F_{wall,j} \times I_{T\,j,t} + \sum_{j\in J} \tau_{win} \times SC \times F_{win,j} \times I_{T\,j,t} + \dot{Q}_{in,t} - \dot{Q}_{EC,t} \Big] - \rho C V (T_{in,t+1} - T_{in,t}) = 0\,, \quad \forall\, t \in T \tag{22}$$

(4) Technical constraints from the EC:

The constraint for the cooling output of EC is shown in Eq. (23):

$$0 \leqslant Q_{EC,t} \leqslant \overline{Q}_{EC}\,, \quad \forall\, t \in T \tag{23}$$

(5) Indoor temperature set-point constraint:

$$\underline{T_{in}} < T_{in,t} < \overline{T_{in}}\,, \quad \forall\, t \in T \tag{24}$$

(6) Electric power purchase constraint:

$$\underline{P_{ex}} < P_{ex,t} < \overline{P_{ex}}\,, \quad \forall\, t \in T \tag{25}$$

2.4.3. Microgrid energy management: stage 2

- *Objective function*

The energy management system runs the stage 2 dispatch problem to smooth the fluctuations of the electric power exchanges at the PCC. Then, the stage 2 dispatch problem is solved to make the actual electric power exchanges at the PCC follow the day-ahead set-points. The dispatch objective over the n_2 time slots without the V2B control is formulated in Eq. (26). The V2B control strategy over the n_3 time slots is described in the following text.

$$\min \{ \left[P_{ex,t'} - P_{ex,t'}^{set} \right]^2 \}\,, \quad \forall\, t' \in T' \tag{26}$$

$P_{ex,t'}^{set}$ is the day-ahead set-point of the electric power exchange at the PCC in time slot t', which is generated in stage 1; $P_{ex,t'}$ is the actual electric power exchange at the PCC in time slot t' of stage 2. The constraints of the dispatch problem over the n_2 time slots are the same as Eqs. (20)–(25).

- *V2B control strategy*

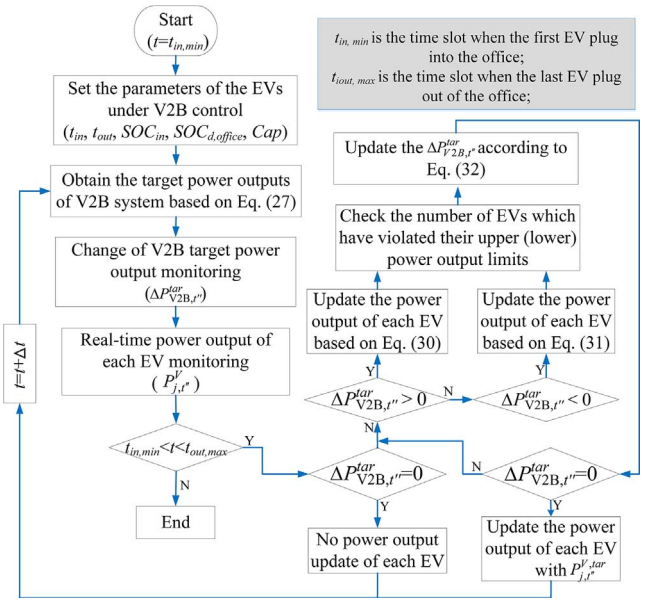

Fig. 4. Flowchart of the V2B control strategy.

The V2B system is dispatched at the stage 2 over the n_3 time slots to further smooth the fluctuations of the electric power exchanges at the PCC. Firstly, solve the stage 2 dispatch problem to obtain the V2B control signals over the n_3 time slots (i.e., the target power output of the V2B system, $P^{tar}_{V2B,t''}$). The dispatch objective over the n_3 time slots with the V2B control is formulated in Eq. (27). Then, the control signals are issued to all the EVs to update their power outputs.

$$\min\{[P_{ex,t''}-P^{set}_{ex,t''}]^2\}, \quad \forall\, t'' \in T'' \tag{27}$$

$P^{set}_{ex,t''}$ is the day-ahead set-point of the electric power exchange at the PCC in time slot t'', which is generated in stage 1; $P_{ex,t''}$ is the actual electric power exchange at the PCC in time slot t'' of stage 2. The constraints consist of Eqs. (20)–(25) and (28).

$$P^{lower}_{V2B,t''} \leqslant P^{tar}_{V2B,t''} \leqslant P^{upper}_{V2B,t''} \tag{28}$$

The upper boundary ($P^{upper}_{V2B,t''}$) and the lower boundary ($P^{lower}_{V2B,t''}$) of the $P_{V2B,t''}$ are updated in every time slot after the V2B control, which is introduced in the following text. The initial boundaries (when t'' = 1) are obtained based on the V2B model without V2B control. Based on the updated upper and lower boundary of the $P_{V2B,t''}$, the energy management system solves the stage 2 dispatch problem in every time slot to generate the $P^{tar}_{V2B,t''}$ in 1 min.

In order to realize the target power output of the V2B system ($P^{tar}_{V2B,t''}$) under the V2B control, the power output of the V2B system ($P_{V2B,t''}$) after V2B control should follow the $P^{tar}_{V2B,t''}$. Then, all the power outputs of the EVs are dispatched considering their operation constraints, as discussed in Section 2.3.3. Thus, the target power output change of the V2B system is determined by Eq. (29).

$$\Delta P^{tar}_{V2B,t''} = P^{tar}_{V2B,t''}-P_{V2B,t''} \tag{29}$$

Then, if $\Delta P^{tar}_{V2B,t''}$ is equal to zero, there is no need to adjust the power output of any EV. Otherwise, the following steps are conducted to determine the updated power output of each EV in the V2B control:

Step (1) If $\Delta P^{tar}_{V2B,t''}$ is higher than zero, the target power output of each EV is determined by Eq. (30). And $m_{1,t}$ is defined as the number

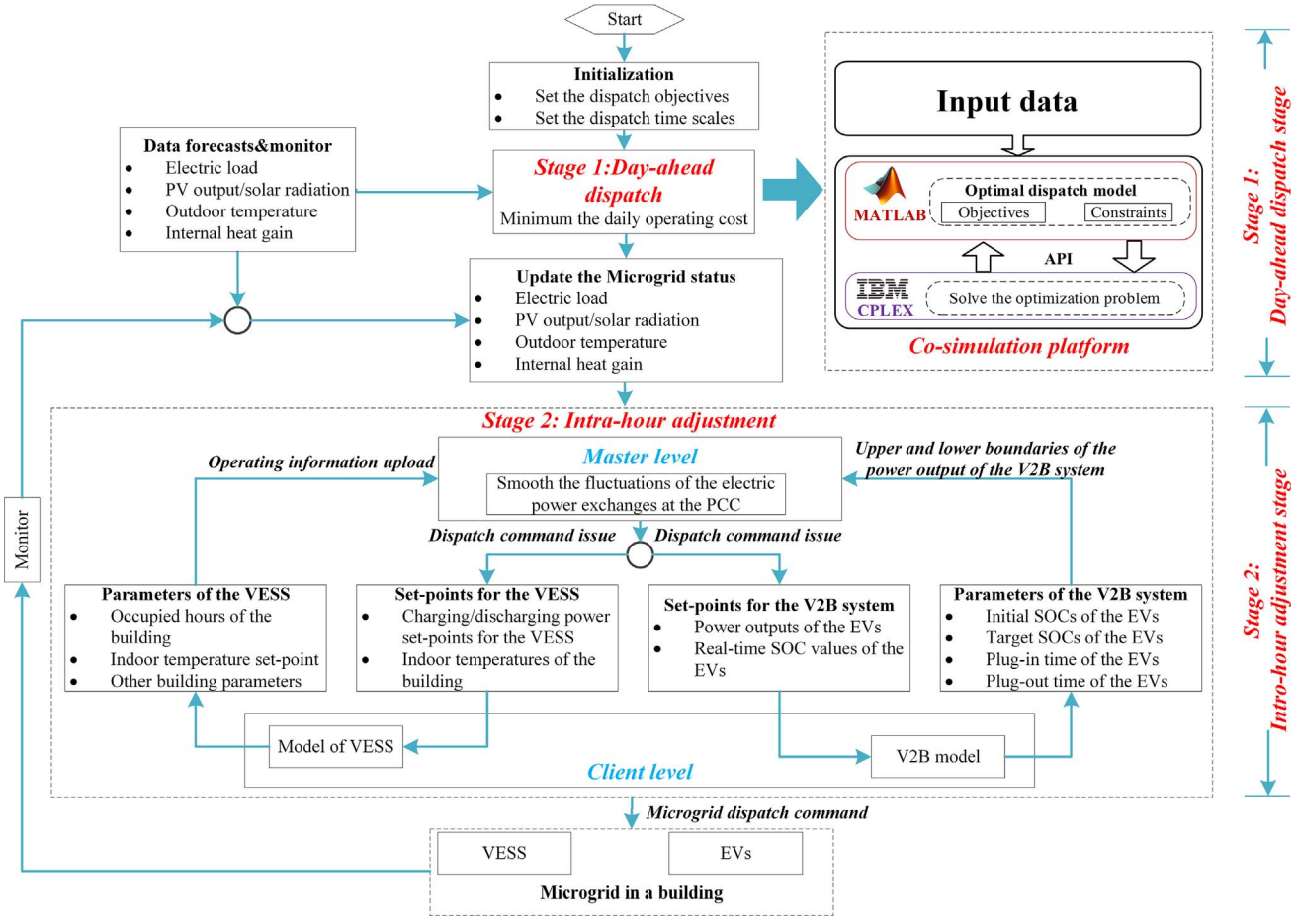

Fig. 5. Flowchart of the hierarchical Microgrid energy management.

of EVs of the V2B system which have not reached their upper limits of power output, i.e. $P^{V}_{j,t''} < \overline{P}^{V}_{j,t''}$. It is clear from Eq. (30) that the EV with higher SOC level will contribute more discharging power to the positive $\Delta P^{tar}_{V2B,t''}$ value.

$$P^{V,tar}_{j,t''} = P^{V}_{j,t''} + \Delta P^{tar}_{V2B,t''} \times \frac{SOC^{V}_{j,t''} - \underline{SOC}^{V}_{j}}{\sum_{j=1}^{m_{1,t}} (SOC^{V}_{j,t''} - \underline{SOC}^{V}_{j})} \tag{30}$$

Step (2) If $\Delta P^{tar}_{V2B,t''}$ is lower than zero, the target power output of each EV is determined by Eq. (31). And $m_{2,t}$ is defined as the number of EVs in the V2B system which have not reached their lower limits of power output, i.e. $P^{V}_{j,t''} > \overline{P}^{V}_{j,t''}$. It is clear from Eq. (31) that the EV with lower SOC level will contribute more charging power to the negative $\Delta P^{tar}_{V2B,t''}$ value.

$$P^{V,tar}_{j,t''} = P^{V}_{j,t''} + \Delta P^{tar}_{V2B,t''} \times \frac{\overline{SOC}^{V}_{j} - SOC^{V}_{j,t''}}{\sum_{j=1}^{m_{2,t}} (\overline{SOC}^{V}_{j} - SOC^{V}_{j,t''})} \tag{31}$$

Step (3) Based on the obtained target power output of each EV, $m_{3,t}$ ($m_{4,t}$) is defined as the number of EVs which have violated their upper (lower) power output limits. Thus, the new revised $\Delta P^{tar}_{V2B,t''}$ is determined by Eq. (32). If $\Delta P^{tar}_{V2B,t''}$ is equal to zero, the power output of EV j after V2B control is updated with $P^{V,tar}_{j,t''}$. If $\Delta P^{tar}_{V2B,t''}$ is not equal to zero, Step 1) ~ Step 3) will be implemented again until the updated $\Delta P^{tar}_{V2B,t''}$ is equal to zero.

$$\begin{cases} \Delta P^{tar}_{V2B,t''} = \sum_{j=1}^{m_{3,t}} (P^{V,tar}_{j,t''} - \overline{P}^{V}_{j,t''}), \quad m_{3,t} > 0 \quad \& \quad m_{4,t} = 0; \\ \Delta P^{tar}_{V2B,t''} = \sum_{j=1}^{m_{4,t}} (P^{V,tar}_{j,t''} - \underline{P}^{V}_{j,t''}), \quad m_{3,t} = 0 \quad \& \quad m_{4,t} > 0. \end{cases} \tag{32}$$

The flowchart of the V2B control strategy is shown in Fig. 4. All the schedules of the EVs are constrained within the operation area, as introduced in Section 2.3.3.

2.4.4. Implementation of the hierarchical management method

The proposed energy management method is described as follows (shown in Fig. 5):

Step (1) (Microgrid initialization): Set the dispatch objectives and time scales for VESS and V2B system. The objective function is to minimize the daily Microgrid operating cost for stage 1; the objective function is to smooth the fluctuations of the electric power exchanges at the PCC for stage 2. Different dispatch intervals are set for the VESS (short dispatch interval in 15 min) and the V2B system (ultra-short dispatch interval in 1 min).

Step (2) (Stage 1: Day-ahead dispatch): Given the day-ahead electric load demand, outdoor temperature, solar radiation and the renewable generation data of the Microgrid (hourly forecasting), the day-ahead dispatch results are obtained by calling the optimal dispatch program in stage 1, as shown in Eq. (19).

Step (3) (Update Microgrid status): Update Microgrid status with short-term forecasting data (intra-hour forecasting) and actual measured data.

Step (4) (Stage 2: Intra-hour adjustment, including dispatch of the VESS and the V2B system): A two-layered dispatch method is proposed to smooth the fluctuations of the electric power exchanges at the PCC. The schedules of the VESS studied in this paper are charging/discharging power for the VESS and the indoor temperature set-points rather than the number and behaviour of the occupants. The schedules of the V2B system studied in this paper are power outputs of all the plug-in EVs and their real-time SOC values rather than the number of plug-in EVs. Their schedules are flexible and can be optimized by the proposed energy management method.

A two-layer solution method is designed and implemented in stage 2 to smooth the fluctuations of the electric power exchanges at the PCC in both short term (15 min) and ultra-short term (1 min). The specific solution method for stage 2 is illustrated as follows:

At the master level, the main dispatch tasks are:

- For the VESS, the optimal dispatch program is used to generate set-points for VESS over the n_2 time slots based on the day-ahead electric power dispatch results and short-term forecasting input data, as shown in Eq. (26);
- For the V2B system, the optimal dispatch program is used to generate the target power outputs of the V2B system over the n_3 time slots based on the day-ahead electric power dispatch results and actual measured data, as shown in Eq. (27).

At the client level, the main dispatch tasks are:

- For the VESS, on one hand, update the schedules of the VESS (the charging/discharging power of the VESS) over the n_2 time slots and upload the updated schedules to the energy management system; On the other hand, upload the operation information (occupied hours of the building and indoor temperature comfort zone) to the master level.
- For the V2B system, on one hand, update the schedules of the EVs (the power outputs of the EVs) over the n_3 time slots and broadcast the updated schedules to the energy management system; On the other hand, generate the upper boundary ($P^{upper}_{V2B,t''}$) and the lower boundary ($P^{lower}_{V2B,t''}$) of the $P_{V2B,t''}$ in every time slot based on the V2B model and V2B control strategy and upload the boundaries to the master level for the optimal dispatch program.

In this paper, the optimal dispatch problem was implemented using IBM ILGO CPLEX on the MATLAB platform [40–42], as shown in Fig. 5. In stage 1, MATLAB routes the optimization model (as shown in Eqs. (19)–(25)) to the solver – IBM ILOG CPLEX Optimizer to solve the optimal dispatch problem. Then, the optimal day-ahead dispatch results are returned to MATLAB for energy management in stage 1. In stage 2, MATLAB routes the short term optimization model (as shown in Eq. (26) and Eqs. (20)–(25)) and the ultra-short term optimization model (as shown in Eq. (27) and Eqs. (20)–(25)) to the solver – IBM ILOG CPLEX Optimizer to solve the optimal dispatch problem. Then, the optimal schedules for the VESS in short term over the n_2 time slots and V2B system in the ultra-short term over the n_3 time slots are returned to MATLAB for energy management in stage 2. The number and behaviour of the occupants affect the electric load and internal heat gain of the building [43]. The number of plug-in EVs determines the adjustable capacity of the V2B system, as illustrated in Section 2.3.3. The electric load and internal heat gain of the building as well as the adjustable capacity of the V2B system are used as input data for the energy management of the office building to generate the flexible schedules of the VESS and the V2B system, as shown in Fig. 5.

3. Results and discussion

3.1. Case study

A Microgrid in a low energy office building shown in Fig. 1 is used to verify the effectiveness of the developed energy management method. The low energy office building with eco-building design (e.g., high performance glazing, energy-saving lighting, etc.) has relative low electric loads and internal heat gains. The building is represented by a parallelepiped with a squared floor. The thermal parameters of the building are given in Table 3 [25]. The occupied hours are set to be from 8:00 a.m. to 20:00 p.m [44]. The values of the parameters of the air mass density ρ and air specific heat ratio C are set to be 1.2 kg/m^3

Table 3
Building parameters [25].

U_{wall} [W/(m^2·K)]	F_{wall} (m^2)	U_{win} [W/(m^2·K)]	Window to wall ratio (%)	Long side (m)	Short side (m)	Height (m)
0.908	2400	2.750	75	40	20	30

and 1000 J/(kg °C) respectively [45,46]. The thermal comfort level for human occupancy depends on environmental factors of temperature, humidity and air speed and personal factors of clothing and metabolic rate [47,48]. Therefore, the acceptable indoor temperature set-point range for human occupancy in an office building varies under different operational scenarios. In this study, the indoor temperature set-point is set to be 19 °C without VESS being dispatched. The indoor temperature set-point range is set to be from 19 °C to 26 °C with VESS being dispatched. It is worth noting that the proposed method is not limited to this temperature set-point range. By setting different comfort zones, it can be applied at both hot climate and cold climate areas. In future, we will extend the proposed energy management method to different indoor temperature ranges.

The electric load and internal heat gain of the building as well as other input data can be predicted in stage 1 and measured in stage 2. Since the V2B system is only committed and dispatched in stage 2, there is no need to predict the number of plug-in EVs in stage 1. The number of plug-in EVs in stage 2 can be monitored and measured by the energy management system thanks to the information and communication technology of the smart office building. The forecasted and actual outdoor temperature in a summer day are shown in Fig. 6 [25]. The forecasted and actual solar radiation on horizontal surface [49] are shown in Fig. 7. The corresponding incident solar radiation on the walls/windows surface at south, west, north and east orientations are calculated based on the method presented by Duffie and Beckman [33], which is used in the model of VESS. The hourly forecasted solar radiation on horizontal surface and calculated incident solar radiation on the walls/windows surface at south, west, north and east orientations are shown in Fig. 8. The rated power of photovoltaic system is 100 kW and the hourly forecasted peak generation by the photovoltaic system is 46 kW. The forecasted and actual electric loads and internal heat gains of the low energy building in a typical summer day are shown in Figs. 9 and 10 respectively. Many researchers focused on load demand, photovoltaic generation and outdoor temperature forecast methodologies. Due to the focus of this paper is not the forecast method, we consider the forecasting errors of all the data in this paper follows the Normal distribution [50]. It is worth noting that both the actual outdoor temperature data and the internal heat gain data are in 15 min because the VESS is dispatched every 15 min at the intra-hour stage. An hourly electricity purchasing price is used in day-ahead optimal dispatch stage [51], as shown in Fig. 11. The price for selling electricity back to the external grid is set to be 0.8 times the price for purchasing electricity [52].

Since the number of plug-in EVs in stage 2 is monitored and measured by the energy management system of the office building, the number of EVs varies under different operational scenarios. The number of EVs is assumed be 10 in this case study. The rated charging and discharging power of an individual EV is 3.3 kW [22]. The other parameters, such as the charging and discharging efficiencies, the plug-in/plug-out time, and the lower and upper limits of SOC are shown in Table 4 [37].

3.2. Day-ahead dispatch results

The day-ahead dispatch schedules of the Microgrid with VESS (the indoor temperature set-point is adjusted within the customer temperature comfort ranges) and without VESS (keep the indoor temperature set-point at the desired value) are shown in Fig. 12. It can be observed that the indoor temperature set-points are adjusted within the comfort range (19–26 °C) during the occupied hours by introducing VESS to the day-ahead optimal dispatch stage. In that case, the daily operating cost of the Microgrid is reduced from $197.2 to $169.2, which is reduced by 14.2%. It can be concluded that the VESS dispatch can reduce the daily operating cost of the Microgrid with limited modifications on the Microgrid management system.

The day-ahead dispatch results of the VESS, the cooling demand of the building with ($\dot{Q}_{cl,building,t}$) and without ($\dot{Q}'_{cl,building,t}$) VESS are shown in Fig. 13. When $\dot{Q}_{cl,building,t}$ is larger than $\dot{Q}'_{cl,building,t}$, the VESS operates in charging mode; when $\dot{Q}_{cl,building,t}$ is smaller than$\dot{Q}'_{cl,building,t}$, the VESS operates in discharging mode. The dispatch results of VESS show that the VESS can be charged or discharged according to the optimal dispatch of the Microgrid. The dispatch results also show that the VESS tends to operate in discharging mode to reduce the daily operating cost. However, due to the constraint of the indoor temperature set-point and energy dissipation characteristics of the building, the VESS is charged after discharging for several time intervals, as shown in Fig. 13.

The relationship between dispatch results of VESS and the electricity prices at the day-ahead dispatch stage is shown in Fig. 14. The VESS is discharged with higher power during high electricity purchase price periods (e.g. 15:00) to reduce the cooling demand and save cost. In order to obtain the high discharging power, the VESS is charged with high power before the discharging process to storage enough cooling power (e.g. 14:00).

3.3. Intra-hour adjustment results

In this case, three comparative scenarios are employed to verify the effectiveness of the proposed energy management method at the intra-hour stage.

3.3.1. VESS dispatch results

Scenario I (reference case): Dispatch the Microgrid with Day-ahead programming (DA-P) method [25] at the intra-hour adjustment stage. Mismatches between the energy demand and supply caused by day-ahead forecasting errors are balanced by the external grid, without short-term dispatch of the VESS.
Scenario II: Dispatch the Microgrid with short-term dispatch of the VESS at the intra-hour adjustment stage. The VESS is dispatched to smooth the electric power fluctuations at the PCC caused by day-ahead forecasting errors.

The electric power set-points at the PCC obtained at the day-ahead dispatch stage discussed in Section 2.4.2 is shown by the black solid line in Fig. 15. The comparative dispatch results in Scenario I (represented by the orange solid line in Fig. 15) and Scenario II (represented by the grey solid line in Fig. 15) suggest that the fluctuations of the electric

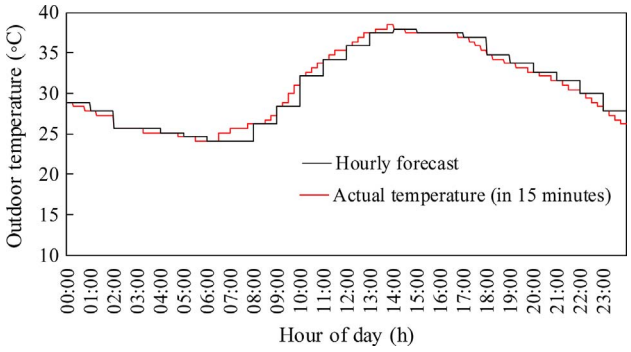

Fig. 6. Outdoor temperature data.

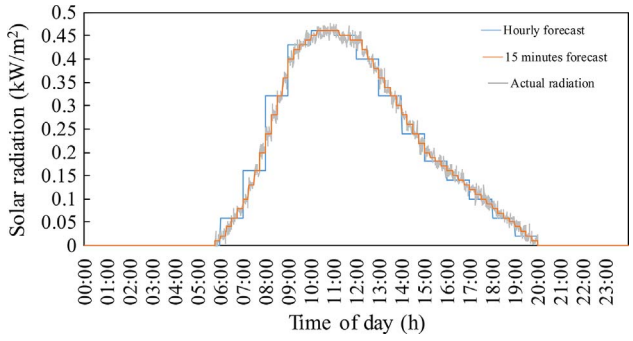

Fig. 7. Solar radiation on horizontal surface.

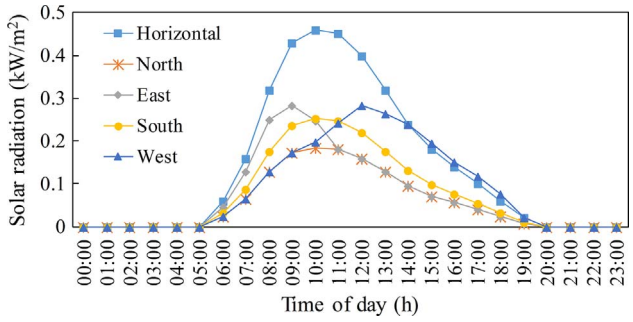

Fig. 8. Hourly forecasted values of incident solar radiation flux.

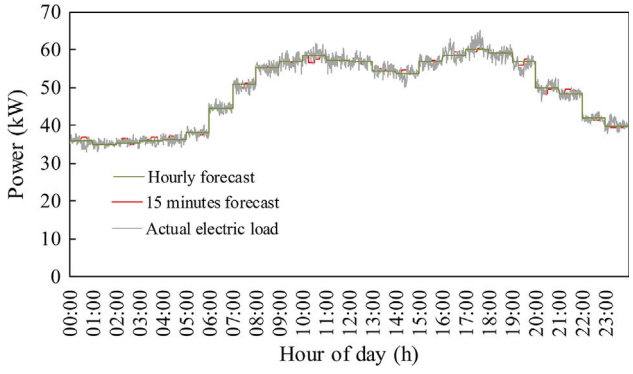

Fig. 9. Electric load of the Microgrid.

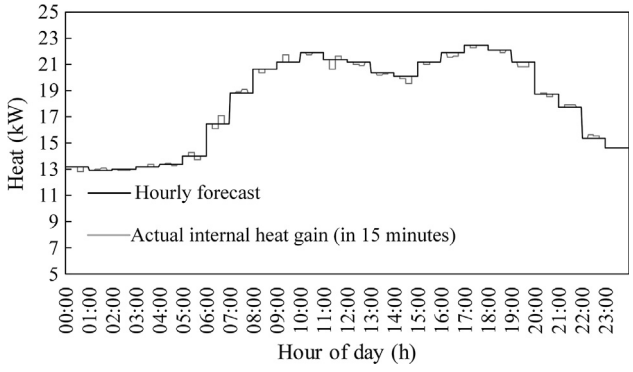

Fig. 10. Internal heat gain of the building.

power exchanges at the PCC can be reduced to some extend using the short-term dispatch of VESS. Since all the mismatches between the energy demand and supply are balanced by electric power from the external grid under the DA-P method in Scenario I, all the forecasting errors are mainly reflected in the electric power fluctuations at the PCC, as shown in Fig. 15. It is worth noting that electric power fluctuations

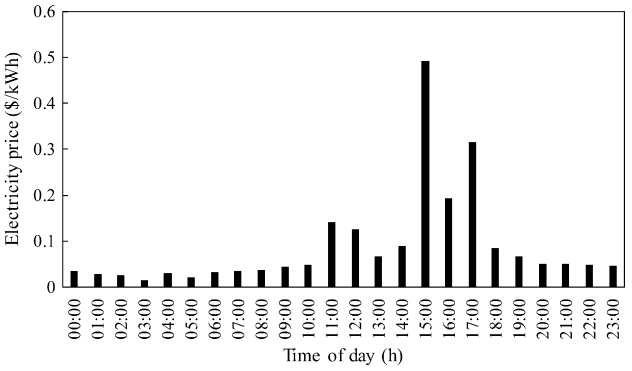

Fig. 11. Real-time electricity purchasing price.

Table 4
EVs parameters [37].

Parameters	Value
$\eta_{c,j}$	0.93
$\eta_{d,j}$	0.93
$t^V_{j,in}$	N (8, 0.25^2)
$t^V_{j,out}$	N (20, 0.25^2)
$\underline{SOC}^V_j$	20%
$\overline{SOC}^V_j$	90%

still exist after the short-term dispatch of the VESS due to the 15 min forecasting errors.

As shown in the circled areas in Fig. 16, there are some large electric power fluctuations at the PCC in some time slots under the DA-P method in Scenario I. This is because that the indoor temperature set-point schedules are generated hourly at the day-ahead stage, while the indoor temperature set-point schedules are implemented every 15 min at the intra-hour stage. Since the mismatches between the energy demand and supply are balanced by electric power from the external grid without short-term dispatch of the VESS under the DA-P method in Scenario I, the intra-hour indoor temperature set-points should be kept the same with the day-ahead indoor temperature set-point schedules. Therefore, when the indoor temperature set-points change in some hourly time slots at the day-ahead stage (as shown in the shaded areas in Fig. 16), more/less electric power is consumed by the EC to follow the changed day-ahead hourly indoor temperature set-points in just 15 min at the intra-hour stage. And the increased/decreased power consumption of the EC are reflected in the large electric power fluctuations at the PCC, as shown in Fig. 16. This means that the changes of indoor temperature set-points during the occupied hours act as triggers for the large electric power fluctuations at the PCC.

Taking the fluctuation of electric power exchange at the PCC at 10:00 as an example, the day-ahead indoor temperature set-point schedules at 9:00 and 10:00 are 26 °C and 19 °C respectively and the corresponding electric power consumptions of EC are 66.15 kW and 100.64 kW, as shown in Fig. 12(a). This means that the indoor temperature set-point drops from 26 °C to 19 °C with 34.49 kW more power consumption of EC in one hour. While at the intra-hour stage in Scenario I, in order to keep the same indoor temperature set-point with the day-ahead indoor temperature set-point schedules, the indoor temperature set-point drops from 26 °C at 9:45 to 19 °C at 10:00 in just 15 min. In this case, more electric power should be consumed by the EC to manage that according to the building thermal equilibrium equation. The electric power consumptions of EC are 71.80 kW and 142.68 KW at 9:45 and 10:00 respectively at the intra-hour stage in Scenario I, as shown in Fig. 17. This means that the indoor temperature set-point drops from 26 °C to 19 °C with 70.88 kW more power consumption of

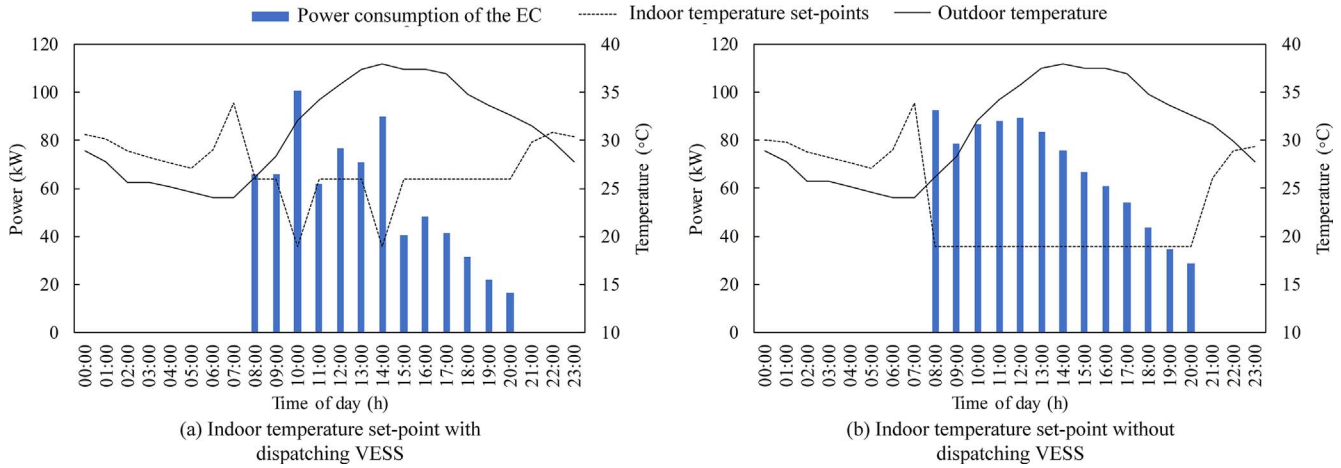

Fig. 12. Day-ahead dispatch schedules of the EC and indoor temperature set-points.

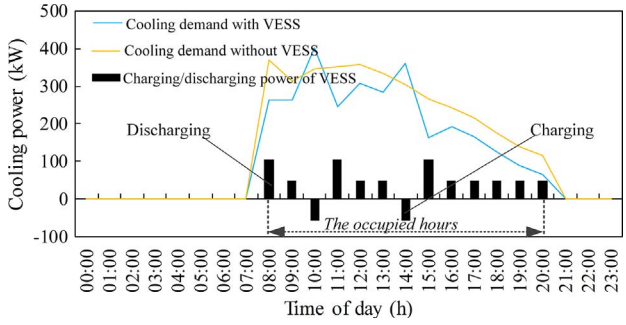

Fig. 13. Dispatch results of the VESS at the day-ahead stage.

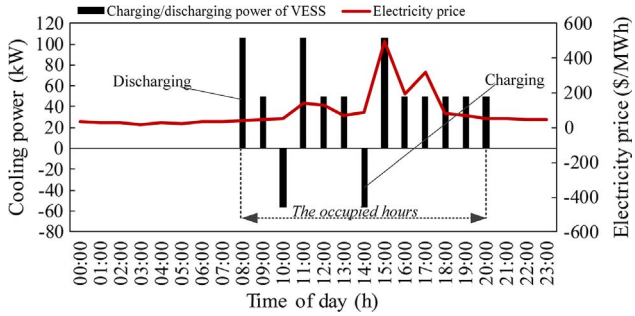

Fig. 14. Relationship between dispatch results of VESS and electricity price.

EC in 15 min, which causes the large fluctuation of electric power exchange at the PCC at 10:00.

With the short-term dispatch of VESS in Scenario II, the large electric power fluctuations at the PCC are reduced, as shown in Fig. 15.

In order to reduce the large electric power fluctuation at the PCC at the beginning of occupied hours in Scenario II, i.e., reduce the electric power consumption of the EC at 8:00, the pre-cooling technique is considered for scheduling the EC [53]. In this case, the EC is started in advance of the occupied hours to storage cooling energy before the occupied hours and the VESS is dispatched in advance as well, as shown in Fig. 15.

It can be observed from Fig. 17 that the indoor temperature set-points of the building and the corresponding power consumption schedules of the EC are adjusted to smooth the fluctuations of electric power exchanges at the PCC. The short-term dispatch results of the VESS in Scenario II, the cooling demand of the building with ($\dot{Q}_{cl,building,t}$) and without ($\dot{Q}'_{cl,building,t}$) VESS are shown in Fig. 18. Compared to the day-ahead dispatch results of the VESS in Fig. 12(a), it can be observed that the schedules of the VESS (the charging/discharging power of the VESS) are updated at the intra-hour stage.

The dispatch results of the cooling demand with indoor temperature set-point of the Microgrid in Scenario I and Scenario II at the intra-hour adjustment stage are depicted in Fig. 19. The comparison dispatch results in Scenario I and Scenario II suggest that the cooling demand and indoor temperature set-point schedules have been updated in Scenario II to dispatch the VESS for smoothing the fluctuations of the electric power at the PCC. The indoor temperature set-point schedules fluctuate within the indoor temperature set-point comfort range (19–26 °C) during the occupied hours in Scenario II. The indoor temperature set-point schedules keep the same with the day-ahead indoor temperature set-points (shown in Fig. 12(a)) during the occupied hours under the DA-P method in Scenario I. Furthermore, the EC is started in advance to storage cooling energy before the occupied hours and the VESS is dispatched in advance in Scenario II as discussed above.

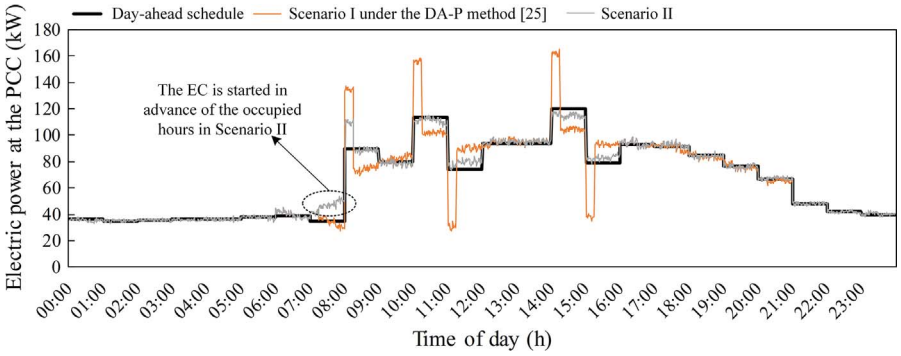

Fig. 15. Electric power exchanges at the PCC of the Microgrid.

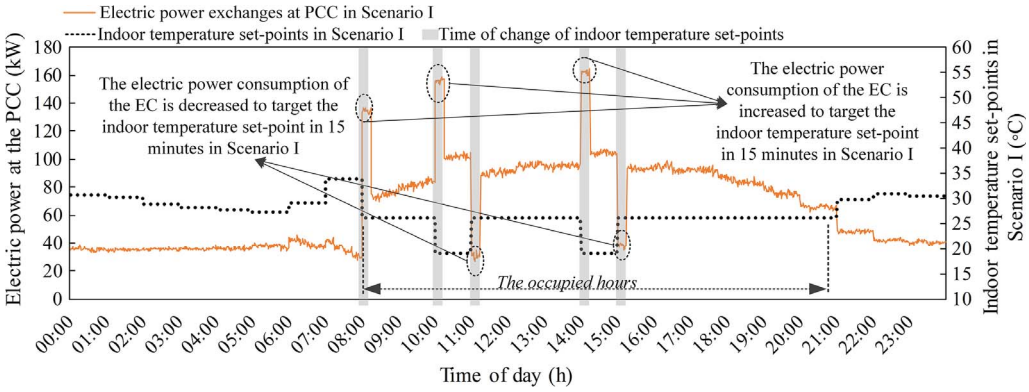

Fig. 16. Electric power exchanges at the PCC and the indoor temperature set-points in Scenario I.

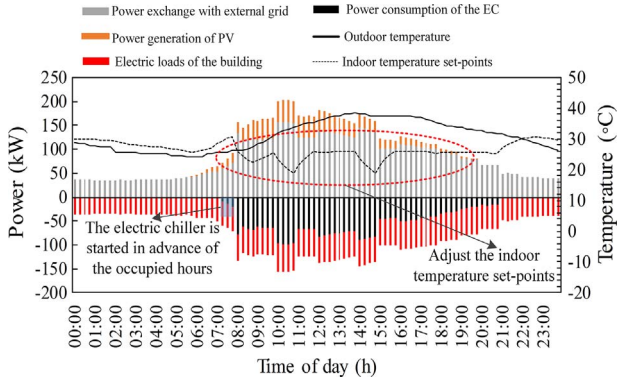

Fig. 17. The short-term dispatch results of the Microgrid with VESS being considered.

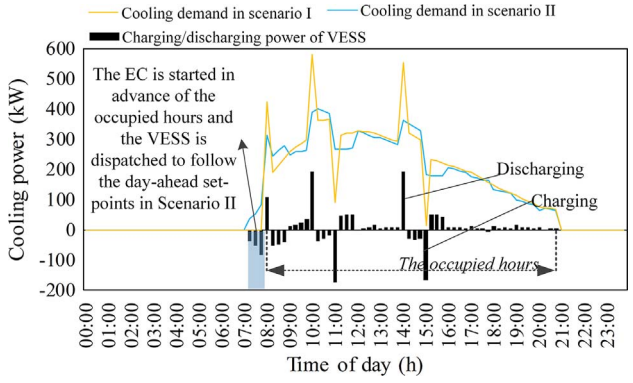

Fig. 18. The short-term dispatch results of the VESS in Scenario II.

3.3.2. V2B dispatch results

As previously mentioned, the V2B system is dispatched in ultra-short term to further smooth the fluctuations of the electric power exchanges at the PCC in stage 2. Scenario III is further developed to verify the effectiveness of the energy management method with ultra-short term dispatch of the V2B system.

Scenario III: Further smooth the fluctuations of the electric power at the PCC by dispatching the V2B system in 1 min.

As introduced in Section 2.4.3, the energy management method in stage 2 is implemented to generate the target power output of the V2B system (represented by the grey solid line in Fig. 20) based on the updated upper boundary (represented by the black solid line in Fig. 20) and the lower boundary (represented by the green solid line in Fig. 20) of the real-time power output of the V2B system. And the target power output of the V2B system is broadcasted to the EVs in every 1 min. Then, all the EVs update their power outputs according to the target power output of the V2B system and the V2B control strategy.

The simulation results shown in Fig. 20 reveal that the V2B system is dispatched within the V2B power output limits. And the real-time power output of the V2B system (represented by the red solid line in Fig. 20) can track the real-time target power output of the V2B system. It is worth noting that due to the EVs are forced to charge with the rated charging power during 19:00–21:00 to guarantee sufficient energy for EV user's travel from work to home at their plug-out times, the V2B power output boundaries are narrowed during 19:00–21:00. Consequently, the expected power output of the V2B system (obtained based on the mismatches between the energy demand and supply after the short-term dispatch of the VESS in Scenario II) cannot be targeted during 19:00–21:00, as represented by the blue solid line in Fig. 20.

A comparison of the dispatch results in Scenario III with forced charging of the EVs (blue solid line in Fig. 21), Scenario I (orange solid

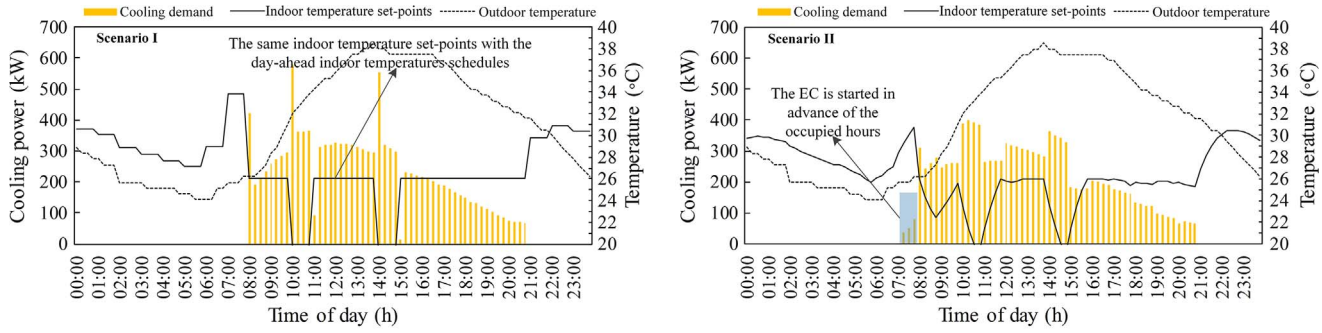

(a) Cooling demand and indoor temperature set-points in Scenario I

(b) Cooling demand and indoor temperature set-points in Scenario II

Fig. 19. The short-term dispatch results of the cooling demand with indoor temperature set-points of the Microgrid at the intra-hour stage.

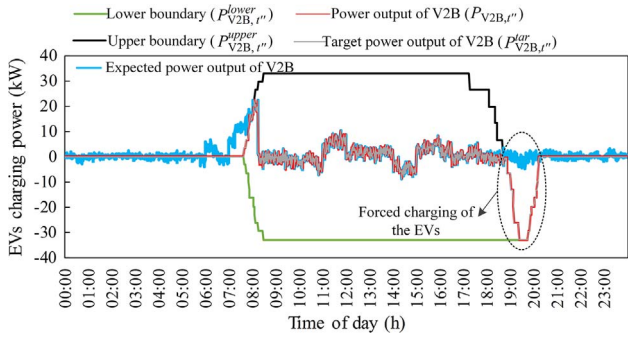

Fig. 20. The ultra-short term dispatch results of the V2B system with forced charging of the EVs.

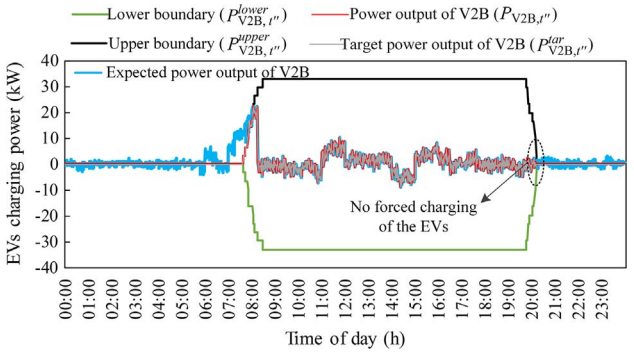

Fig. 22. The ultra-short term dispatch results of the V2B system without forced charging of the EVs.

line in Fig. 21) and Scenario II (grey solid line in Fig. 21) suggests that the electric power fluctuations at the PCC are well smoothed by the V2B system. The fluctuations shown in the circled area in Fig. 21 are due to the forced charging loads of the EVs, as discussed above. The electric power exchanges at the PCC in Scenario III without forced charging of the EVs (red solid line in Fig. 21) show that the circled fluctuations can be well smoothed without considering the forced-charging boundary in the V2B control. Consequently, the expected power output of the V2B system can be targeted and the real-time power output of the V2B system can also track the real-time target power output of the V2B system, as shown in Fig. 22.

To further validate the effectiveness of the proposed method, the mean square errors (MSEs) of the electric power exchange at the PCC under three scenarios are compared [54], as shown in Eq. (33). The day-ahead set-points of the electric power exchange at the PCC are used as reference values.

$$\begin{cases} MSE_I = \sqrt{\frac{1}{t''}\sum_{t''=1}^{n_3}(P^{I}_{ex,t''}-P^{set}_{ex,t''})^2} \\ MSE_{II} = \sqrt{\frac{1}{t''}\sum_{t''=1}^{n_3}(P^{II}_{ex,t''}-P^{set}_{ex,t''})^2} \\ MSE_{III} = \sqrt{\frac{1}{t''}\sum_{t''=1}^{n_3}(P^{III}_{ex,t''}-P^{set}_{ex,t''})^2} \\ MSE_{III^*} = \sqrt{\frac{1}{t''}\sum_{t''=1}^{n_3}(P^{III^*}_{ex,t''}-P^{set}_{ex,t''})^2} \end{cases} \quad (33)$$

$P^{I}_{ex,t''}$, $P^{II}_{ex,t''}$, $P^{III}_{ex,t''}$ and $P^{III^*}_{ex,t''}$ are the electric power exchange at the PCC under Scenario I, Scenario II, Scenario III with forced charging of the EVs and Scenario III without forced charging of the EVs respectively. The MSEs denote the sample standard deviation between the values under different scenarios and reference values. The smaller value of MSE denotes that the fluctuations of the electric power exchanges at the PCC is better smoothed. The values of MSE under different scenarios are shown in Table 5.

The comparative results shown in Figs. 15, 21 and Table 5 demonstrate that fluctuations of the electric power exchanges at the PCC can be well smoothed by the proposed method with short-term dispatch of the VESS and ultra-short term dispatch of the V2B system.

Table 5
MSEs under different scenarios.

Scenario	MSE
I under the DA-P method [25]	11.53
II	5.99
III with force charging of the EVs	3.95
III without force charging of the EVs	1.99

A comparison of the real-time SOC values of the EVs in Scenario III with/without forced charging suggests that all the EVs can be charged to their minimum expected SOC values when they leave the office (shown in Fig. 23) considering the forced-charging boundary in the V2B control. Otherwise, the EVs cannot be charged to their minimum expected SOC values. Since the office hour is from 8:00 a.m. to 20:00 p.m [44], most of the EVs arrive at the office at around 8:00 am and most of them leave the office at round 20:00 pm, as shown in Fig. 23. The plug-in time and plug-out time are different among the EVs.

4. Conclusion

This paper proposes a hierarchical Microgrid energy management method in an office building by dispatching two flexible energy resources, i.e. the VESS and the V2B system. Optimal dispatch schedules are generated for the Microgrid at the day-ahead dispatch stage to reduce the daily operating cost. For the intra-hour adjustment stage, a two-layered approach is designed to smooth the fluctuations of the electric power exchanges at the PCC, taking the uncertainties from the renewable generation, electric load demand, outdoor temperature and the solar radiation into account. To incorporate the different response characteristics and the forecasting errors of the input data at different time scales, the VESS and the V2B system are coordinated at two

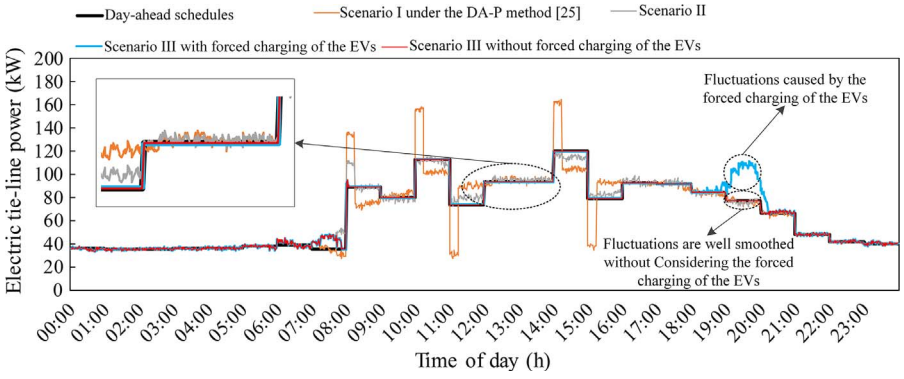

Fig. 21. Electric power exchanges at the PCC of the Microgrid in the comparative scenarios.

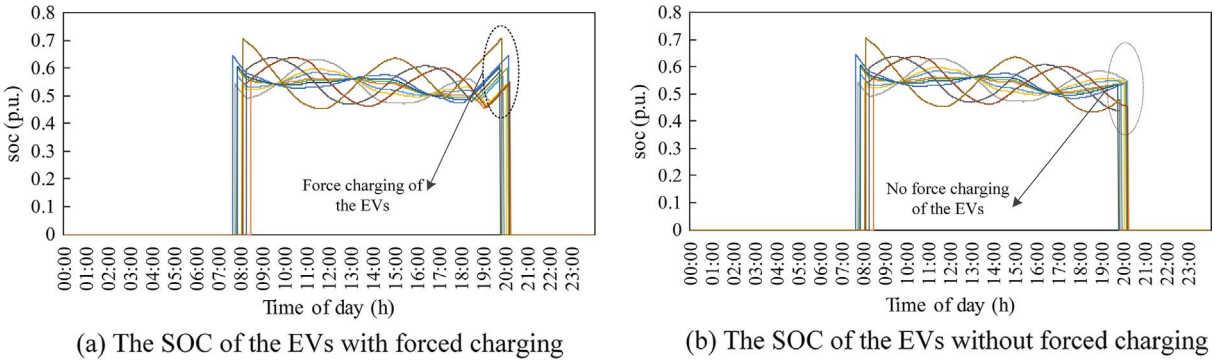

Fig. 23. The real-time SOC values of the EVs at the intra-hour adjustment stage.

different time scales. At the master level, the VESS is dispatched within a short-term. A V2B control strategy is further developed to dispatch the power output of the V2B system within an ultra-short term. At the client level, the operation information of the VESS as well as the upper and lower boundaries of the V2B system are generated and uploaded to the master level. Numerical studies show that the proposed energy management method can reduce the daily operating cost and smooth the fluctuations of the electric power exchanges at the PCC. It is also shown that the two flexible resources (the VESS and the EVs) can be dispatched under appropriate control strategies according to the energy management demand of the Microgrid. Meanwhile, the customers' temperature comfort level and travelling demands can be maintained. Furthermore, the proposed energy management method can also be used to meet other requirements for the Microgrid, such as minimizing the energy emissions, shifting the HBW EVs' charging loads to the office building while improving the renewable energy self-consumption capability of the office building.

Acknowledgements

This work was financially supported by the National High-tech R & D Program of China (863 Program with No. 2015AA050403), the project National Natural Science Foundation of China (Grant Nos. 51677124 and 51625702). This research is also partially funded by the MISTRAL project (Grant No. EP/N017064/1) and the FLEXIS project. FLEXIS is part-funded by the European Regional Development Fund (ERDF), through the Welsh Government. Information on the data that underpin the results presented here, including how to access them, can be found in the Cardiff University data catalogue at http://doi.org/10.17035/d.2017.0041619600.

References

[1] Keirstead J, Jennings M, Sivakumar A. A review of urban energy system models: approaches, challenges and opportunities. Renew Sust Energ Rev 2012;16(6):3847–66.
[2] Wu J, Yan J, Jia H, et al. Integrated energy systems. Appl Energy 2016;167:155–7.
[3] International Energy Agency. Energy technology perspectives 2012: pathways to a clean energy system. Paris (France); 2012.
[4] The European Parliament. Directive 2010/31/EU of the European Parliament and the Council on 19 May 2010 on the Energy Performance of Buildings (recast). Off. J. Eur. Union 2010;153:13–35.
[5] Amecke H, Deason J, Hobbs A, et al. Buildings energy efficiency in China, Germany, and the United States. Climate Policy Initiative; 2013.
[6] Efficient Building Advocates, Meet China. The Institute for Building Efficiency. http://www.institutebe.com/energy-policy/efficiency-building-advocates-meet-china.aspx.
[7] Yu J, Tian L, Xu X, et al. Evaluation on energy and thermal performance for office building envelope in different climate zones of China. Energy Build 2015;86:626–39.
[8] Bin S, Jun L. Building energy efficiency policies in China: status report. Glob Build Perform Netw 2012.
[9] Diamond RC, Ye Q, Feng W, et al. Sustainable building in China—a green leap forward. Buildings 2013;3(3):639–58.
[10] Li DHW, Chow SKH, Lee EWM. An analysis of a medium size grid-connected building integrated photovoltaic (BIPV) system using measured data. Energy Build 2013;60(5):383–7.
[11] Guan X, Xu Z, Jia QS. Energy-efficient buildings facilitated by microgrid. IEEE Trans Smart Grid 2010;1(1):243–52.
[12] Zhang D, Shah N, Papageorgiou LG. Efficient energy consumption and operation management in a smart building with microgrid. Energy Convers Manage 2013;74(74):209–22.
[13] Yang H, Pan H, Luo F, et al. Operational planning of electric vehicles for balancing wind power and load fluctuations in a microgrid. IEEE Trans Sustain Energy 2016. http://dx.doi.org/10.1109/TSTE.2016.2613941.
[14] Xu X, Jin X, Jia H, et al. Hierarchical management for integrated community energy systems. Appl Energy 2015;160:231–43.
[15] Zhang D, Evangelisti S, Lettieri P, et al. Economic and environmental scheduling of smart homes with microgrid: DER operation and electrical tasks. Energy Convers Manage 2016;110(Suppl4):113–24.
[16] Zhao Y, Lu Y, Yan C, et al. MPC-based optimal scheduling of grid-connected low energy buildings with thermal energy storages. Energy Build 2014;86:415–26.
[17] Lu Y, Wang S, Sun Y, Yan C. Optimal scheduling of buildings with energy generation and thermal energy storage under dynamic electricity pricing using mixed-integer nonlinear programming. Appl Energy 2015;147:49–58.
[18] Wang Z, Wang L, Dounis AI, et al. Integration of plug-in hybrid electric vehicles into energy and comfort management for smart building. Energy Build 2012;47:260–6.
[19] Wang Y, Wang B, Chu CC, et al. Energy management for a commercial building microgrid with stationary and mobile battery storage. Energy Build 2016;116:141–50.
[20] Mu Y, Wu J, Ekanayake J, Jenkins N, Jia H. Primary frequency response from electric vehicles in the Great Britain power system. IEEE Trans Smart Grid 2013;4(2):1142–50.
[21] Meng J, Mu Y, Jia H, et al. Dynamic frequency response from electric vehicles considering travelling behavior in the Great Britain power system. Appl Energy 2016;162:966–79.
[22] Van Roy J, Leemput N, Geth F, et al. Electric vehicle charging in an office building microgrid with distributed energy resources. IEEE Trans Sustain Energy 2014;5(4):1–8.
[23] Nguyen HK, Song JB. Optimal charging and discharging for multiple PHEVs with demand side management in vehicle-to-building. J Commun Netw-s KOR 2012;14(6):662–71.
[24] Moroşan PD, Bourdais R, Dumur D, et al. Building temperature regulation using a distributed model predictive control. Energy Build 2010;42(9):1445–52.
[25] Jin X, Mu Y, Jia H, et al. Dynamic economic dispatch of a hybrid energy microgrid considering building based virtual energy storage system. Appl Energy 2017;194:386–98.
[26] Bitar EY, Rajagopal R, Khargonekar PP, et al. Bringing wind energy to market. IEEE Trans Power Syst 2012;27(3):1225–35.
[27] Rosa MD, Bianco V, Scarpa F, et al. Heating and cooling building energy demand evaluation; a simplified model and a modified degree days approach. Appl Energy 2014;128:217–29.
[28] Cristofari C, Norvaišienė R, Canaletti JL, Nottona G. Innovative alternative solar thermal solutions for housing in conservation-area sites listed as national heritage assets. Energy Build 2015;89:123–31.
[29] Yang IH, Yeo MS, Kim KW. Application of artificial neural network to predict the optimal start time for heating system in building. Energ Convers Manage 2003;44(17):2791–809.
[30] ISO 13790:2008. Energy performance of buildings–calculation of energy use for space heating and cooling; 2008.
[31] ISO 6946:2007. Building components and building elements–thermal resistance and thermal transmittance–calculation method; 2007.
[32] Ozel M, Pihtili K. Optimum location and distribution of insulation layers on building walls with various orientations. Build Environ 2007;42(8):3051–9.
[33] Duffie JA, Beckman WA. Solar engineering of thermal process. New York: Wiley; 1991.
[34] Zainal OA, Yumrutaş R. Validation of periodic solution for computing CLTD (cooling load temperature difference) values for building walls and flat roofs. Energy 2015;82:758–68.
[35] Mu Y, Wu J, Jenkins N, et al. A spatial–temporal model for grid impact analysis of plug-in electric vehicles. Appl Energy 2014;114:456–65.

[36] EU Merge Project. Deliverable 2.1: Modelling electric storage devices for electric vehicles; 2010. [Online]. Available: http://www.ev-merge.eu/images stories/uploads/MERGE_WP2_D2.1.pdf.
[37] Wang M, Mu Y, Jia H, et al. Active power regulation for large-scale wind farms through an efficient power plant model of electric vehicles. Appl Energy 2017;185:1673–83.
[38] Dong X, Yunfei MU, Jia H, et al. Planning of fast EV charging stations on a round freeway. IEEE Trans Sustain Energy 2016;7(4):1452–61.
[39] Zhong J, He L, Li C, et al. Coordinated control for large-scale EV charging facilities and energy storage devices participating in frequency regulation. Appl Energy 2014;123:253–62.
[40] IBM ILOG CPLEX Optimization Solver 12.2.
[41] Zhang N, Kang C, Xia Q, et al. A convex model of risk-based unit commitment for day-ahead market clearing considering wind power uncertainty. IEEE Trans Power Syst 2014;30(3):1582–92.
[42] Su W, Wang J, Zhang K, et al. Model predictive control-based power dispatch for distribution system considering plug-in electric vehicle uncertainty. Elect Power Syst Res 2014;106(1):29–35.
[43] D'Oca S, Hong T, Langevin J. The human dimensions of energy use in buildings: a review. Renew Sust Energ Rev 2018;81:731–42.
[44] Ardeshir M, Abdolazim M, Elham K, et al. Occupants' operation of lighting and shading systems in office buildings. J Build Perform Simu 2008;1(1):57–65.
[45] Singh AK, Tiwari GN, Lugani N, et al. Energy conservation in a cinema hall under hot and dry condition. Energy Convers Manage 1996;37(5):531–9.
[46] Mui KW. Energy policy for integrating the building environmental performance model of an air conditioned building in a subtropical climate. Energy Convers Manage 2006;47(15–16):2059–69.
[47] ISO Standard 7730. Moderate thermal environments – determination of the PMV and PPD indices and specification of the conditions for thermal comfort. Geneva: International Organisation for Standardisation; 1994.
[48] ASHRAE Standard 55P. Thermal environmental conditions for human occupancy. Atlanta (USA): American Society of Heating, Refrigerating and Airconditioning Engineers; 2003.
[49] Kaşka Önder. Yumrutaş R. Experimental investigation for total equivalent temperature difference (TETD) values of building walls and flat roofs. Energy Convers Manage 2009;50(11):2818–25.
[50] Zhang Y, Zhang T, Wang R, et al. Optimal operation of a smart residential microgrid based on model predictive control by considering uncertainties and storage impacts. Sol Energy 2015;122:1052–65.
[51] Mandal P, Haque AU, Meng J, et al. A novel hybrid approach using wavelet, firefly algorithm, and fuzzy artmap for day-ahead electricity price forecasting. IEEE Trans Power Syst 2013;28(2):1041–51.
[52] Zhang Y, Wang R, Zhang T, et al. Model predictive control-based operation management for a residential microgrid with considering forecast uncertainties and demand response strategies. IET Gener Transm Dis 2016;10(10):2367–78.
[53] Haniff MF, Selamat H, Yusof R, et al. Review of HVAC scheduling techniques for buildings towards energy-efficient and cost-effective operations. Renew Sust Energ Rev 2013;27(8):94–103.
[54] Ghasemi A, Shayeghi H, Moradzadeh M, et al. A novel hybrid algorithm for electricity price and load forecasting in smart grids with demand-side management. Appl Energy 2016;177:40–59.